Overview

Residual stress
Part 1 – Measurement techniques

P. J. Withers and H. K. D. H. Bhadeshia

Residual stress is that which remains in a body that is stationary and at equilibrium with its surroundings. It can be very detrimental to the performance of a material or the life of a component. Alternatively, beneficial residual stresses can be introduced deliberately. Residual stresses are more difficult to predict than the in-service stresses on which they superimpose. For this reason, it is important to have reliable methods for the measurement of these stresses and to understand the level of information they can provide. In this paper, which is the first part of a two part overview, the effect of residual stresses on fatigue lifetimes and structural integrity are first summarised, followed by the definition and measurement of residual stresses. Different types of stress are characterised according to the characteristic length scale over which they self-equilibrate. By comparing this length to the gauge volume of each technique, the capability of a range of techniques is assessed. In the second part of the overview, the different nature and origins of residual stress for various classes of material are examined. MST/4640A

Professor Withers is in the Manchester Materials Science Centre, University of Manchester and UMIST, Grosvenor Street, Manchester M1 7HS, UK (philip.withers@man.ac.uk). Professor Bhadeshia is in the Department of Materials Science and Metallurgy, University of Cambridge, Pembroke Street, Cambridge CB2 3QZ, UK (hkdb@cus.cam.ac.uk). *Manuscript received 3 March 2000; accepted 6 December 2000.*

Introduction

With modern analytical and computational techniques it is often possible to estimate the stresses to which a component is subjected in service. This in itself is not sufficient for the reliable prediction of component performance. Indeed, in many cases where unexpected failure has occurred, this has been due to the presence of residual stresses which have combined with the service stresses to seriously shorten component life. On the other hand, compressive stresses are sometimes introduced deliberately, as in shot peening which is used to improve fatigue resistance. Furthermore, in natural or artificial multiphase materials, residual stresses can arise from differences in thermal expansivity, yield stress, or stiffness. Considerable effort is currently being devoted to the development of a basic framework within which residual stresses can be incorporated into design in aerospace, nuclear, and other critical engineering industries.

The materials scientist and the engineer can now access a large number of residual stress measurement techniques. Some are destructive, while others can be used without significantly altering the component; some have excellent spatial resolution, whereas others are restricted to near-surface stresses or to specific classes of material. In this paper, part 1 of a two part overview, the techniques most commonly used for the characterisation of residual stress are reviewed. In part 2,[1] the nature and the origin of residual stress for different classes of material are described.

Types of stress

Residual stresses in a body are those which are not necessary to maintain equilibrium between the body and its environment. They may be categorised by cause (e.g. thermal or elastic mismatch), by the scale over which they self-equilibrate, or according to the method by which they are measured. In this paper, a length scale perspective is adopted. As illustrated in Fig. 1, residual stresses originate from misfits between different regions. In many cases, these misfits span large distances, for example, those caused by the non-uniform plastic deformation of a bent bar. They can also arise from sharp thermal gradients, for example, those caused during welding or heat treatment operations (Fig. 1). Whether mechanically or thermally induced, these stresses can be advantageous, as in the case of shot peening and the toughening of glass.

The macrostresses just described are of type I because they vary continuously over large distances (Fig. 2). This is in contrast to residual stresses which vary over the grain scale (type II or intergranular stresses) or the atomic scale (type III). In these cases, the misfitting regions span microscopic or submicroscopic dimensions. Low level type II stresses nearly always exist in polycrystalline materials simply from the fact that the elastic and thermal properties of differently oriented neighbouring grains are different. More significant grain scale stresses occur when the microstructure contains several phases or phase transformations take place. The type III category typically includes stresses due to coherency at interfaces and dislocation stress fields.

Since the techniques available sample a variety of length scales, they may record different stress values. Figure 2 illustrates how the different types of stress equilibrate over different length scales $l_{0,\mathrm{I}}$, $l_{0,\mathrm{II}}$, and $l_{0,\mathrm{III}}$. For a two phase material, the macrostress is continuous across phases, but the type II and III stresses are not. As a result, even when the sampling area is greater than the characteristic areas for type II and type III, non-zero phase-average microstresses $\langle\sigma_1\rangle_{\mathrm{A}}^{\mathrm{II,III}}$ and $\langle\sigma_2\rangle_{\mathrm{A}}^{\mathrm{II,III}}$ can be recorded. Considering the stresses in the z direction

$$0=\int_{\mathrm{A}}\sigma_{zz}\{x,y\}\,\mathrm{d}A_z$$

$$=\int_{\mathrm{A_1}}\sigma_{zz}\{x,y\}^{\mathrm{II}}\,\mathrm{d}A_z+\int_{\mathrm{A_2}}\sigma_{zz}\{x,y\}^{\mathrm{II}}\,\mathrm{d}A_z \quad \ldots \quad (1)$$

$$=f_{\mathrm{A}}\langle\sigma_1\rangle_{\mathrm{A}}^{\mathrm{II}}+(1-f_{\mathrm{A}})\langle\sigma_2\rangle_{\mathrm{A}}^{\mathrm{II}} \quad \ldots \quad (2)$$

where f_{A} and $(1-f_{\mathrm{A}})$ are the area fractions A_1/A and A_2/A respectively. Extending the analysis to three dimensions by

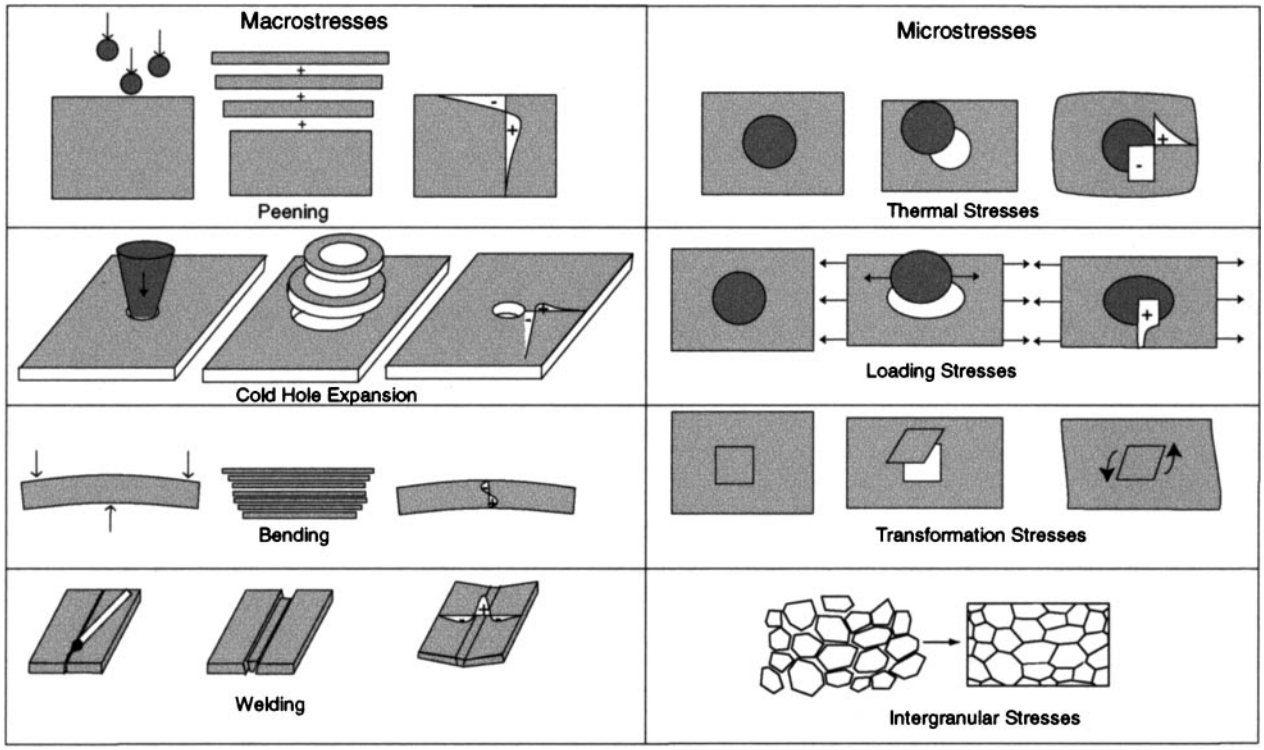

1 Residual stresses arise from misfits (eigenstrains) either between different regions or between different phases within material: different types of residual macro and micro residual stress are illustrated

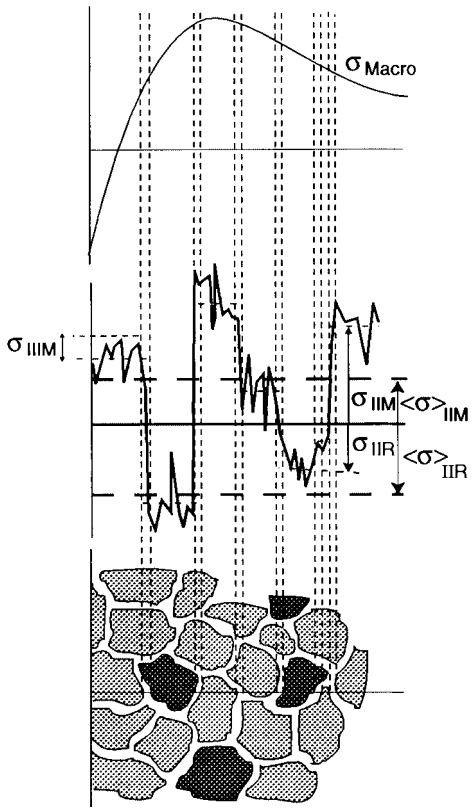

M and R denote matrix and reinforcement respectively

2 Residual stress fields can be categorised according to characteristic length scales $l_{0,I}$, $l_{0,II}$, and $l_{0,III}$ over which they self-equilibrate: for type I, $l_{0,I}$ represents considerable fraction of component; for type II, $l_{0,II}$ is comparable to grain dimensions, while for type III, $l_{0,III}$ is less than grain diameter

integrating over the sampling volume, the type II volume average phase stresses ($\langle\sigma_1\rangle^{II}$ and $\langle\sigma_2\rangle^{II}$) must obey

$$0 = f\langle\sigma_1\rangle^{II} + (1-f)\langle\sigma_2\rangle^{II} \quad \ldots\ldots\ldots (3)$$

if the sampling volume is larger than the characteristic volume for type II. In other words, while the type II and type III stresses must balance over the appropriate small distance, there may be a phase dependent residual effect over large distances; this leads to a mean background stress in each phase.[2] A good example of this is nickel base superalloys with a microstructure of γ' particles in a matrix of γ. Both phases are in the cubic crystal system and indeed in a cube–cube relative orientation, but their lattice parameters do not match exactly. The particles are therefore in forced coherence with the matrix with the coherency strains focused at the interfaces. The lattice parameters of the two phases are slightly different when they are measured for the phases in isolation and when they are combined in the conventional microstructure,[3] i.e. there exist non-zero mean phase type II microstresses.

It is useful to consider the characteristic volume V_0 ($\approx l_0^3$ in most cases)[4] over which a given type of stress averages to zero. If the measurement sampling volume is greater than V_0, then the stress will not be recorded, since it averages to zero over that length scale. For example, most material removal techniques (e.g. hole drilling, layer removal) remove macroscopically sized regions ($V \gg V_{0,II}$, $V_{0,III}$) over which type II and III stresses average to zero so that only the macrostress is recorded. While the sampling volumes typical in diffraction experiments are also larger than $V_{0,II}$, at a given wavelength and (*hkl*) diffraction condition, only a particular phase or grain orientation is sampled. As a consequence a non-zero volume averaged phase microstress $\langle\sigma_1\rangle^{II}$ or grain stress $\langle\sigma_{hkl}\rangle^{II}$ can also be recorded superimposed on the phase independent macrostress (σ^I). Clearly, considerable care must be taken when selecting the most appropriate residual stress measurement technique. It is important to ask what components of the stress tensor, or types of stress, are required by the materials designer to improve performance or for the engineer to make a structural integrity assessment. For example, the

designer of composite materials might be interested in the development of type II volume averaged phase stresses, in order to learn about the transfer of load from the matrix to the reinforcement. In contrast, in the life assessment of metallic components, type II and type III are often unimportant,[1] and attention is focused on type I macrostresses. According to the problem under consideration, this might be the hydrostatic tensile component responsible for creep cavitation, or the mode I crack opening stress component affecting crack growth. As a consequence, unexpected behaviour may not be due to the incorrect measurement of stress but to the measurement of the wrong stress component caused by an inappropriate choice of technique. A few of the more commonly used techniques are summarised in Table 1.

Table 1 Summary of various measurement techniques and their attributes: values of resolution and penetration quoted are broadly representative of technique concerned and $\langle II \rangle$ represents volume averaged type II stresses

Method	Penetration	Spatial resolution	Accuracy	Comments
Hole drilling (distortion caused by stress relaxation)	$\sim 1{\cdot}2\times$ hole diameter	50 μm depth	± 50 MPa, limited by reduced sensitivity with increasing depth	Measures in-plane type I stresses; semidestructive
Curvature (distortion as stresses arise or relax)	0·1–0·5 of thickness	0·05 of thickness; no lateral resolution	Limited by minimum measurable curvature	Unless used incrementally, stress field not uniquely determined; measures in-plane type I stresses
X-ray diffraction (atomic strain gauge)	<50 μm (Al); <5 μm (Ti); <1 mm (with layer removal)	1 mm laterally; 20 μm depth	± 20 MPa, limited by non-linearities in $\sin^2\psi$ or surface condition	Non-destructive only as a surface technique; sensitive to surface preparation; peak shifts: types I, $\langle II \rangle$; peak widths: type II, III
Hard X-rays (atomic strain gauge)	150–50 mm (Al)	20 μm lateral to incident beam; 1 mm parallel to beam	$\pm 10\times10^{-6}$ strain, limited by grain sampling statistics	Small gauge volume leads to spotty powder patterns; peak shifts: type I, $\langle II \rangle$, II; peak widths: types II, III
Neutrons (atomic strain gauge)	200 mm (Al); 25 mm (Fe); 4 mm (Ti)	500 μm	$\pm 50\times10^{-6}$ strain, limited by counting statistics and reliability of stress free references	Access difficulties; low data acquisition rate; costly; peak shifts: type I, $\langle II \rangle$ (widths rather broad)
Ultrasonics (stress related changes in elastic wave velocity)	>10 cm	5 mm	10%	Microstructure sensitive; types I, II, III
Magnetic (variations in magnetic domains with stress)	10 mm	1 mm	10%	Microstructure sensitive; for magnetic materials only; types I, II, III
Raman	<1 μm	<1 μm approx.	$\Delta\lambda \approx 0{\cdot}1$ cm$^{-1} \equiv 50$ MPa	Types I, II

Effects of residual stress

While it is not the aim here to review the effects of residual stress on performance in detail, it is important to consider briefly the reasons why residual stress is measured at all.

The static loading performance of brittle materials can be improved markedly by the intelligent use of residual stress. Common examples include thermally toughened glass and prestressed concrete. In the former, rapid cooling of the glass from elevated temperature generates compressive surface stresses counterbalanced by tensile stresses in the interior. The surface compressive stress (~ 100 MPa) means that the surface flaws that would otherwise cause failure at very low levels of applied stress experience in-plane compression. While the interior experiences counterbalancing tensile stresses, this region is largely defect free and so the inherent strength of the glass is sufficient to prevent failure. Of course, once a crack does penetrate the interior which is under tension, it can grow rapidly and catastrophically go give the characteristic shattered 'mosaic' pattern. In fact, it is possible to assess the original residual stress from the scale of the mosaic pattern. Like glass, concrete is brittle and hence has a low tensile strength. Concrete can nevertheless be used in tension, as in cantilever beams, when it is prestressed in compression. Considerable applied tensile stresses can then be tolerated before the superposition of the applied and residual stresses lead to a net tension of the concrete.

For plastically deformable materials, the residual and applied stresses can only be added together directly until the yield strength is reached. In this respect, residual stresses may accelerate or delay the onset of plastic deformation; however, their effect on static ductile failure is often small because the misfit strains are small and so are soon washed out by plasticity.

The effects of residual stresses on fatigue lifetimes are covered in detail elsewhere.[5] Residual stress can raise or lower the mean stress experienced over a fatigue cycle. It is possible to quantify the effect on life using the Gerber or Goodman relations (Fig. 3*a*). From this it can be seen that because a tensile residual stress increases the mean stress, the stress amplitude must be reduced accordingly if the lifetime is to be unaffected. At large mean values, the tensile residual stresses may even trigger static fracture during fatigue. Free surfaces are often a preferred site for the initiation of a fatigue crack. This means that considerable advantage can be gained by engineering a compressive in-plane stress in the near surface region, for example, by peening, autofrettage, cold hole expansion, case hardening, etc. The largest gains are experienced in low amplitude high cycle fatigue, the least in large strain-controlled low cycle fatigue. This is because, in the latter case, initiation is caused by local alternating strains that exceed the yield stress. These plastic strains soon relax or smooth the prior residual

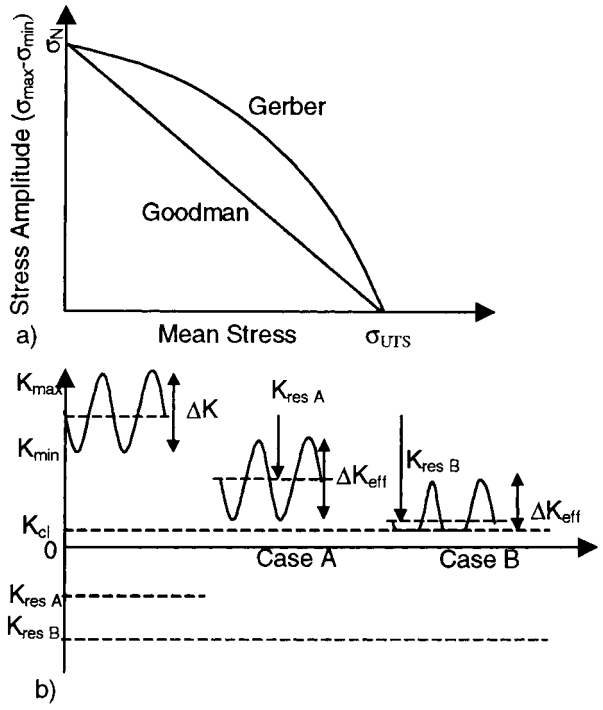

a constant life plot for mean stress versus stress amplitude; *b* effective stress intensity range ΔK_{eff} for two compressive residual stress levels (A, B) with non-zero crack closure stress intensity factor K_{cl}

3 Effect of residual stress on fatigue lifetime

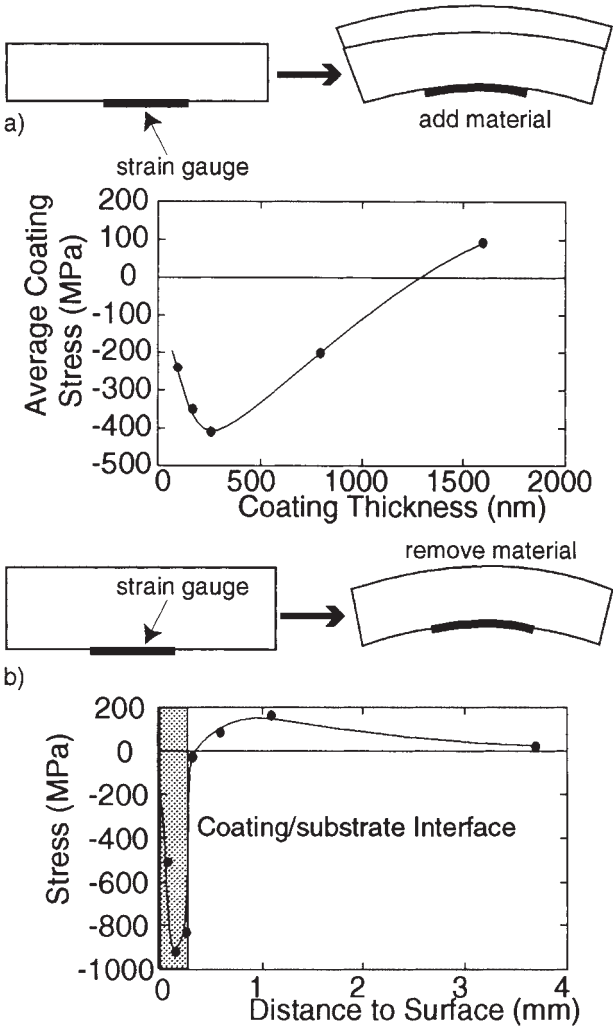

a basis of method for monitoring development of residual stresses during deposition of coating, experimental data were obtained for various thicknesses of sputtered Mo;[9] *b* basis of method for 'post-mortem' deduction of residual stress by layer removal, experimental data obtained for plasma deposited tungsten carbide coating on Ti substrate using layer removal[13]

4 Curvature methods of measuring residual stress

stresses. During fatigue crack growth, the near threshold and high growth rate regimes are strongly affected by mean stress, whereas the Paris regime is insensitive to mean stress. Therefore, unless a change in the mean stress brings about crack closure, residual stresses have little effect on crack growth rates in the Paris regime (Fig. 3*b*). On the whole, type II and type III stresses tend to be washed out by plasticity in the crack tip zone so that only type I stresses need be considered from a fatigue point of view. This is not true for short crack growth which is microstructure and type II stress dependent. Furthermore, type II stresses can be important when considering the fatigue of fibrous composites for which crack bridging can be an important crack retarding mechanism.

Mechanical stress measurement methods

These methods rely on the monitoring of changes in component distortion, either during the generation of the residual stresses, or afterwards, by deliberately removing material to allow the stresses to relax.[6,7]

CURVATURE

Curvature measurements are frequently used to determine the stresses within coatings and layers.[7] The deposition of a layer can induce stresses which cause the substrate to curve,[8] as illustrated in Fig. 4*a*. The resulting changes in curvature during deposition make it possible to calculate the corresponding variations in stress as a function of deposit thickness. Curvature can be measured using contact methods (e.g. profilometry, strain gauges) or without direct contact (e.g. video, laser scanning, grids, double crystal diffraction topology[10]), allowing curvatures down to about 0·1 mm^{-1} to be routinely characterised. Measurements are usually made on narrow strips (width/length $<0{\cdot}2$) to avoid multiaxial curvature and mechanical instability.

The Stoney equation[6] is often used to relate the deflection g of a thin beam of length l and stiffness E to the stress σ along the beam

$$\sigma = -\frac{4}{3} E \frac{h^2}{l^2} \frac{\mathrm{d}g}{\mathrm{d}h} \quad \ldots\ldots\ldots\ldots\ldots (4)$$

where h is the current thickness.

Curvature measurements can also be used 'post-mortem' to determine the stresses by incremental layer removal (Fig. 4*b*). This has been done for metallic[11] and polymeric composites,[12] and for thin coatings produced using plasma or chemical vapour deposition[7,13–15] and physical vapour deposition.[10,16] When incremental layer removal is impractical, it is possible to estimate the in-plane stress levels if assumptions are made about their through thickness distribution. There is some ambiguity in this latter approach, because the stress distribution associated with a given curvature is not unique.

HOLE DRILLING

The undisturbed regions of a sample containing residual stresses will relax into a different shape when the locality is

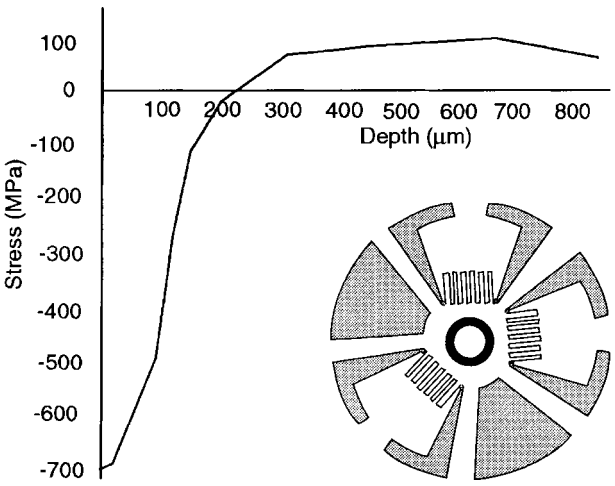

5 Dataset collected for stress in shot peened Ni based alloy using hole drilling method: suitable arrangement of strain gauges is shown inset

machined, thereby providing data for the back-calculation of residual stress. The machining operation usually involves drilling a hole around which the strain is measured using either a rosette of strain gauges (Fig. 5) (e.g. Refs. 17, 18); moire interferometry; laser interferometry based on a rosette of indentations;[19] or holography.[20,21] In general terms

$$\sigma=(\sigma_{max}+\sigma_{min})\ \bar{A}+(\sigma_{max}-\sigma_{min})\ \bar{B}\ \cos\ 2\beta \qquad (5)$$

where $\bar{A}$ and $\bar{B}$ are hole drilling constants, and β is the angle from the x axis to the direction of maximum principal stress, σ_{max}. For the general case of a hole drilled in an infinite plate, $\bar{A}$ and $\bar{B}$ must be calculated numerically.[22]

Although it is possible to deduce the variation in stress with depth by incrementally deepening the hole, it is difficult to obtain reliable measurements much beyond a depth equal to the diameter. (Procedures have been developed to extend the measurement depth.[23]) With a three strain gauge rosette it is only possible to measure the two in-plane components of the stress field. Nevertheless, the method is cheap, widely used and it has been applied even to polymeric samples.[24] Water jets have been used in preference to mechanical drilling to reduce the depth of machining induced deformation.[25] If the residual stresses exceed about 50% of the yield stress, then errors can arise due to localised yielding.[22] While the method has been used to assess the levels of stress in coatings,[26,27] it is not really practical for thin (<100 μm), or for brittle coatings.

COMPLIANCE METHODS

The crack compliance method involves cutting a small slot to monitor the relaxation of stress in the vicinity of the crack using strain gauge interferometry.[28] By steadily increasing the depth of the slot, it is possible to resolve the stress field normal to the crack as a function of depth for relatively simple stress distributions.[29,30] Material can also be removed chemically.[31] A variant of this method has even been used to assess the residual stress state of arteries in rabbits.[32]

Finally, various other removal techniques have been reported.[33] For example, it has also been possible to monitor residual thermal stresses in the fibre phase of a continuous fibre metal matrix composite by etching away the matrix and measuring the change in the fibre length.[34] Another method is based on cutting a section by electro-discharge machining and inferring the prior normal stresses from the deviations from planarity.[35]

Stress measurement by diffraction

Changes in interplanar spacing d can be used with the Bragg equation to detect elastic strain ε through a knowledge of the incident wavelength λ and the change in the Bragg scattering angle $\Delta\theta$

$$\lambda=2d\ \sin\ \theta$$

giving

$$\varepsilon=\frac{\Delta d}{d}=-\cot\ \theta\ \Delta\theta \qquad (6)$$

It is, of course, usually necessary to have an accurate measure of d_0, the stress free spacing. The strain results can then be converted into stress using a suitable value of the stiffness (e.g. *see* Ref. 36).

Because diffraction is inherently selective, and therefore biased towards a particular set of grains, the peak shift will sample both the type I and the average type II stresses for the particular grain set. (The type III stresses simply give peak broadening.) This can be exploited for multiphase materials to provide information about the stressing of the individual phases separately,[37,38] but for single phase materials the intergranular type II stresses mean that the elastic strain recorded for a given reflection may not be representative of the bulk elastic strain. Corrections must be made for the intergranular stresses before the macrostress can be deduced.

In a single phase material, intergranular stresses usually comprise two terms. First, the elastic stiffness mismatch between differently oriented grains can be accounted for by the use of experimentally or theoretically determined diffraction elastic constants (Poisson's ratio ν_{hkl} and elastic modulus E_{hkl}).[39,40] These relate the macrostress to the strain ε_{hkl} recorded normal to the (hkl) planes using the hkl reflection. The second term is due to differences in the plastic yielding response of adjacent grains. While the effect can be accounted for,[40] the simplest solution is to choose reflections which are relatively unaffected by plastic incompatibility intergranular stresses within the material (e.g. *see* Ref. 41).

Using diffraction it is only possible to determine the lattice strain for a given (hkl) plane spacing in the direction of the bisector of the incident and diffracted beams. In order to calculate the stress (or strain) tensor at a sampling gauge location at least six independent measurements of strain in different directions $\varepsilon\{\phi, \psi\}$ are required[42,43]

$$\varepsilon\{\phi,\psi\}=\varepsilon_{11}\ \cos^2\ \phi\ \sin^2\ \psi+\varepsilon_{12}\ \sin\ 2\phi\ \sin^2\ \psi+\varepsilon_{22}\ \sin^2\ \phi\ \sin^2\ \psi+\varepsilon_{33}\ \cos^2\ \psi+\varepsilon_{13}\ \cos\ \phi\ \sin\ 2\psi+\varepsilon_{23}\ \sin\ \phi\ \sin\ 2\psi \qquad (7)$$

$$\sigma_{ij}=C_{ijkl}\varepsilon_{kl}=\frac{E_{hkl}}{1+\nu_{hkl}}\left(\varepsilon_{ij}+\frac{\nu_{hkl}}{1-2\nu_{hkl}}\ \varepsilon_{kk}\delta_{ij}\right) \qquad (8)$$

where C is the stiffness tensor and ψ, ϕ are the polar angles to the tensor coordinate system. In many cases, the principal stress directions can be deduced by symmetry arguments and thus only three strain values are required to calculate the principal stresses

$$\sigma_{11}=\frac{E_{hkl}}{(1-\nu_{hkl})\ (1-2\nu_{hkl})}\times[(1-\nu_{hkl})\ \varepsilon_{11}+\nu_{hkl}(\varepsilon_{22}+\varepsilon_{33})]\quad \text{etc} \qquad (9)$$

In certain cases, even fewer strain measurements are needed, for example, to determine an in-plane biaxial plane stress ($\sigma_{11}=\sigma_{22}$, $\sigma_{33}=0$) only the in-plane strain ε_{11} or the out-of-

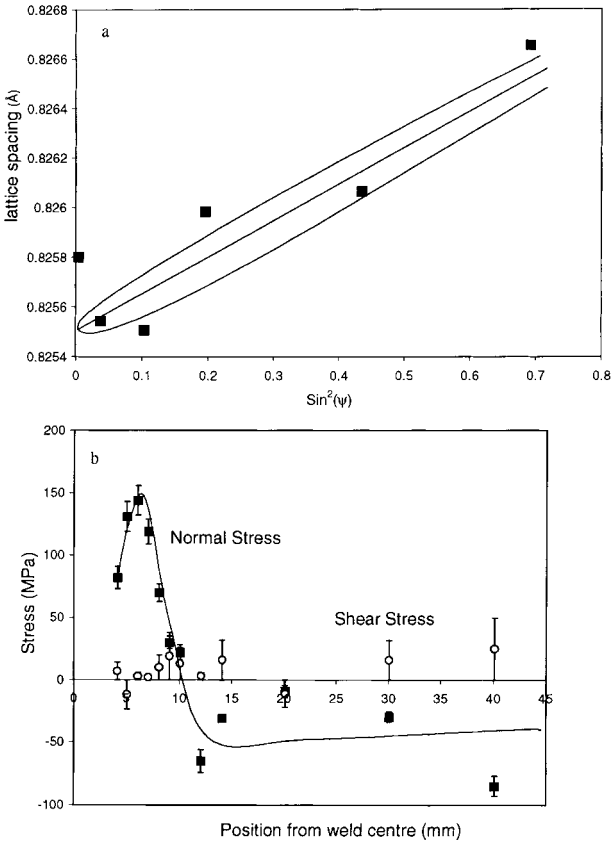

a typical set of Al (422) $\sin^2\psi$ data; *b* results obtained for stress distribution lateral to 8 mm wide tungsten inert gas weld in 3 mm thick plate

6 Measurement of residual strain using X-ray $\sin^2\psi$ method

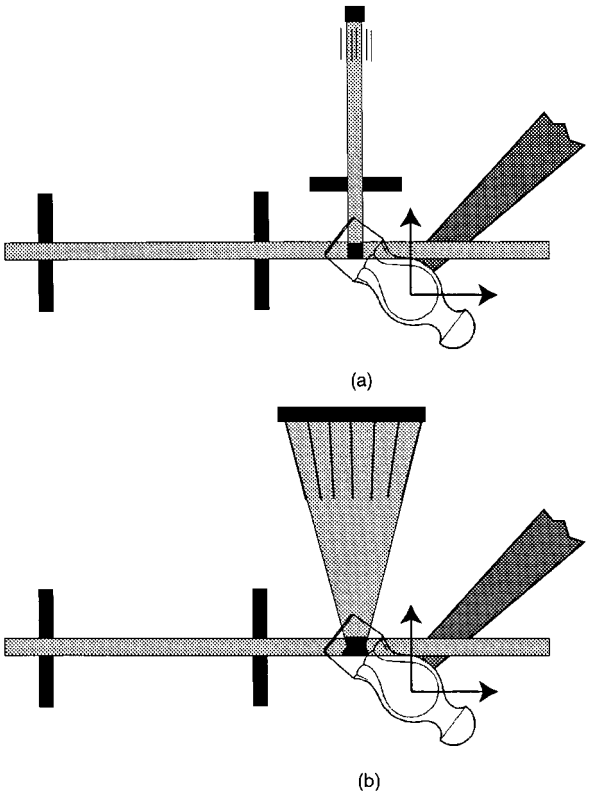

a slits or *b* collimating vanes are used to restrict line of sight of detector to small gauge volume deep within material: to produce strain or stress map, object is stepped systematically through gauge volume; different components of strain tensor are measured by rotating component to relevant angles

7 Definition of neutron sampling volume

plane strain ε_{33} is required

$$\sigma_{11}=\frac{E_{hkl}\varepsilon_{11}}{(1-\nu_{hkl})} \quad \text{or} \quad \sigma_{11}=-\frac{E_{hkl}\varepsilon_{33}}{2\nu_{hkl}}$$

ELECTRON DIFFRACTION

Very high lateral spatial resolution can be achieved using electron beams which can readily be focused to diameters as small as 10 nm. The convergent beam electron diffraction technique is commonly used to achieve the greatest strain resolution.[44] Only very thin samples (<100 nm) can be examined, which naturally renders the results vulnerable to surface relaxation effects and the strain values represent an integral through the thickness. Nevertheless, the method provides a way of measuring type II and type III stresses, such as the misfit strains between γ/γ' phases in nickel superalloys[45–47] and 'macrostresses' in very small electronic device structures.[48]

LABORATORY X-RAY DIFFRACTION

Laboratory ($\lambda\approx0{\cdot}1-0{\cdot}2$ nm wavelength) X-rays probe a very thin surface layer (typically tens of micrometres). This limitation can be used to advantage in the $\sin^2\psi$ technique[39] where the small depth of penetration means that the sampled region can often be assumed to be in plane stress ($\sigma_{3i}=0$ for all i). This obviates the need for an accurate strain free d_0 lattice spacing determination, because, for plane strain, the slope of the measured lattice spacing with specimen tilt ψ can be related directly to the level of in-plane stress σ_{11}

$$\text{slope of } \sin^2\psi \text{ versus } d=\left(\frac{1+\nu_{hkl}}{E_{hkl}}\right)\sigma_{11}d_0 \quad . \quad . \quad . \quad (10)$$

where ν_{hkl} and E_{hkl} are the appropriate diffraction elastic constants for the Bragg reflection used and ψ is the angle between the material surface normal and the bisector of the incident and reflected beams, i.e. the strain measurement direction (Fig. 6).

While the plane stress assumption is true at the surface, its general validity over the sampling depth l depends on the scales and relative magnitudes of the type I and type II components. This assumption is reasonable for systems with macrostresses which tend to vary over large distances compared with the penetration depth, but it is less satisfactory for situations in which there are significant type II stresses. This is because the type II stresses, such as those in composite materials, may equilibrate over very short distances from the free surface depending on the microstructure ($l_{0,II}\approx$interparticle spacing[49]). This complication is discussed for composites in part 2.[1] Good measures of the in-plane macrostress are obtained only when the penetration depth is small compared with the scale of the microstructure. Depth resolved studies can be undertaken using surface removal techniques, but the practical depth limit is really only about 1 mm. Errors can arise when investigating rough surfaces (e.g. welds) using the conventional focusing optics arrangement due to changes in sample 'heights'.

Glancing incidence methods can be used for thinner films and involve a reduction in the depth of penetration by the use of very low incident beam angles (>1°) (e.g. for diamond-like films[50]). At still lower incident angles (<0·5°), total reflection occurs and the X-ray beam forms an

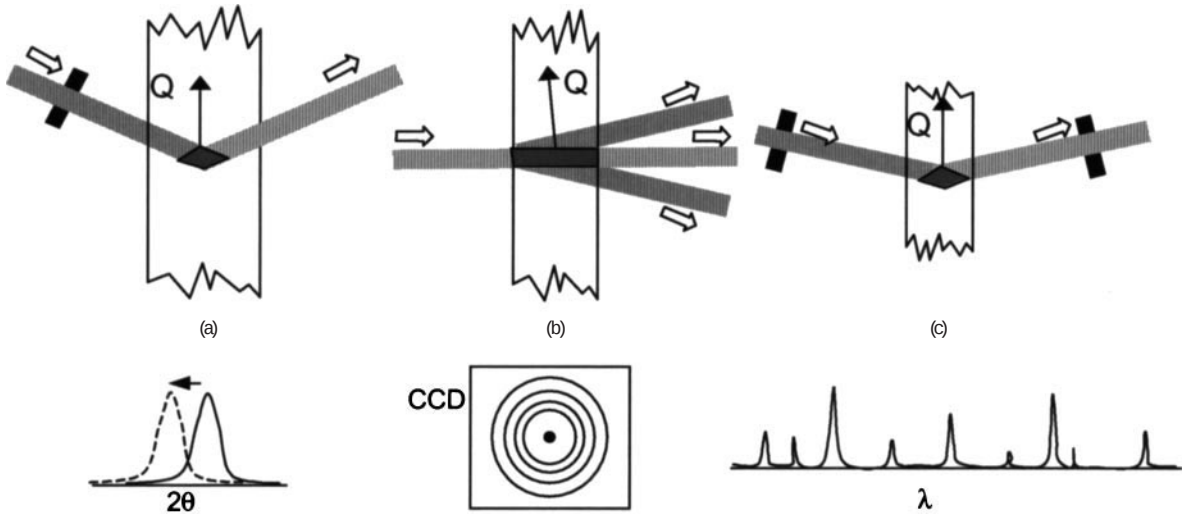

a 2θ scanning; *b* low angle transmission; *c* energy dispersive

8 Schematic illustration of synchrotron measurement geometries

evanescent wave which penetrates a mere 3 nm or so. This is so called grazing incidence diffraction.[51] In this configuration, the detector is positioned at 2θ to the incident beam, but just above the film surface such that the diffracting plane normal lies almost within the surface, thus, it can provide a direct measure of the in-plane strain.

NEUTRONS

Neutrons have the advantage over X-rays that for wavelengths comparable to the atomic spacing, their penetration into engineering materials is typically many centimetres. By restricting the irradiated region and the field of view of the detector by slits or radial collimetors, it is possible to obtain diffracted intensity from only a small volume (>1 mm^3), from deep within a sample (Fig. 7).

There are essentially two neutron diffraction techniques, namely, conventional $\theta/2\theta$ scanning and time of flight approaches. These two methods have developed largely because of the two forms in which neutron beams are available, i.e. either as a continuous beam from a reactor source, or as a pulsed beam from a spallation source. The former is well suited to conventional $\theta/2\theta$ scanning, whereby shifts $\Delta\theta$ in a single hkl diffraction peak are monitored according to equation (6), while the latter is well suited to the time of flight method. In this case, the diffraction profile is not collected as a function of the Bragg angle θ, rather the Bragg angle is held constant (usually $2\theta=90^\circ$) and the incident wavelength λ varied. This is because within each pulse of neutrons leaving the moderated target there is a large range of neutron energies. Naturally, the most energetic neutrons arrive at the specimen first, the least energetic last. Consequently, the energy and hence wavelength of each detected neutron can be deduced from the time that has elapsed since the pulse of neutrons was produced at the target, i.e. from the time of flight. In this case, the strain is given by $\varepsilon=\Delta t/t$, where t is the time of flight. As the strain resolution is dependent upon the accuracy of the measurement of the time of flight, high resolution instruments tend to have large flight paths (>100 m).

The choice between the two neutron diffraction methods can be regarded as a choice between measuring all the diffracting neutrons using a single wavelength with the $\theta/2\theta$ scan, and measuring the diffracting neutrons for all wavelengths for a fraction of the time (i.e. fifty times a second) with the time of flight approach. In general, continuous sources tend to offer the best performance when a small region of the whole diffraction profile is required (e.g. single peak based measurements of the macrostress), while time of flight instruments are especially good in situations where a number of peaks, or the whole diffraction profile, is required (e.g. for multiphase materials or where large intergranular strains are to be expected). At a time of flight instrument, it is most common to use a Rietveld refinement to derive a single value of the lattice spacing by simultaneously fitting a curve to the intensity profile from all the reflections within the time of flight capabilities of the instrument. This value is weighted towards those peaks which are most intense and has been shown both experimentally and theoretically to be a very good representation of the bulk elastic response, relatively insensitive to the tensile and compressive shifts of the various reflections.[52]

An important complication in the application of neutron diffraction is the introduction of apparent strains when

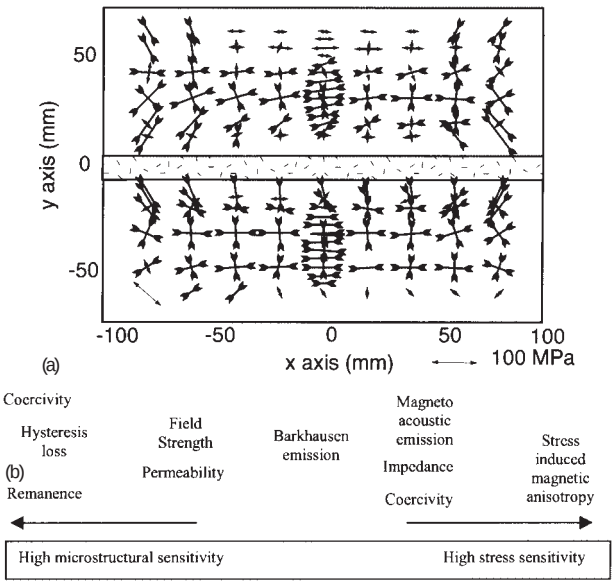

9 *a* stress map collected for welded plate (Courtesy D. Buttle) and *b* sensitivity of various magnetic parameters to stress and microstructure (Courtesy of AEA Technology)

internal or external surfaces are encountered. This arises because of shifts in the centre of gravity of the diffracting volume when it is only partially filled. Provided the diffraction geometry is well known and the attenuation of the diffracting material is included these effects can be accounted for.[53,54] Another approach is to adopt the z scan geometry in which the surface is approached not in the horizontal plane, causing lateral partial filling of the gauge volume, but by bringing the testpiece into the gauge volume vertically causing no lateral displacement of the centre of gravity of the scattering volume and hence no geometrical peak shift.[53]

HARD X-RAYS

Synchrotron (or hard) X-rays are now becoming available at central facilities; synchrotron sources can be as much as a million times more intense than conventional sources and can provide high energy photons (20–300 keV) that are over a thousand times more penetrating than conventional X-rays. Little research has been carried out to date, but very fast data acquisition times (<1 s) using small lateral gauge dimensions (>20 μm) at large depths (as much as 50 mm in aluminium) are possible.[55–58] At least three different methods have been applied to date using

(i) traditional $\theta/2\theta$ methods[57,58] (Fig. 8*a*)
(ii) high energy two-dimensional diffraction[55,59] (Fig. 8*b*)
(iii) white beam high energy photons[60] (energy dispersive method, Fig. 8*c*).

In all cases, the relatively high energies involved lead to very low scattering angles (typically ranging from about 10° at moderate energies (25 keV) to about 4° at high energies (80 keV). This leads to gauge volumes having an elongated diamond shape (typically as little as 20 μm lateral to the beam, but as much as 1 mm along it) and hence poor resolution perpendicular to the scattering vector, i.e. the strain measurement direction (Fig. 8).

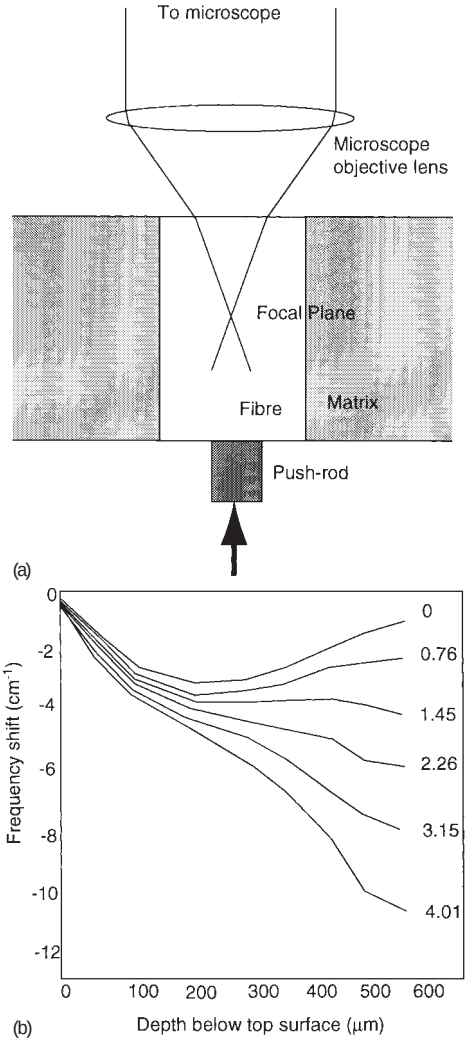

a experimental arrangement for collecting fluorescence data during push-out of fluorescing fibre;[72] *b* variation in frequency shift as push-out load is increased for sapphire fibre with Mo coating in TiAl matrix (shift $\Delta\nu = 5{\cdot}4\sigma_{radial} + 2{\cdot}15\sigma_{axial}$ with $\Delta\nu$ expressed in cm^{-1} and axial and fibre stresses in GPa)

10 Exploiting piezospectroscopic effects to measure residual stress in fibre composites

Other methods

MAGNETIC AND ELECTRICAL TECHNIQUES

When magnetostrictive materials are stressed the preferred domain orientations are altered, causing domains most nearly oriented to a tensile stress to grow (positive magnetostriction) or shrink (negative magnetostriction). Stress induced magnetic anisotropy[61] leads to the rotation of an induced magnetic field away from the applied direction.[62] A sensor coil can monitor these small rotations in the plane of the component surface. When no rotation is observed, the principal axes of the magnetic field and stress are parallel. By rotating the assembly, both the principal stress directions and the size of the principal stress difference can be measured (Fig. 9*a*). Magnetoacoustic emission is the generation of elastic waves caused by changes in magnetostrictive strain during the movement of magnetic domain walls and is generally detected from the material bulk.[63] Barkhausen emission on the other hand, is recorded as a change in the emf proportional to the rate of change in magnetic moment detected in probe coils as domain walls move.[64] It is attenuated at high frequencies by eddy current shielding and so provides only a near surface probe (<250 μm). The largest Barkhausen signal is given by the sudden movement of 180° domains, since this causes the largest change in magnetic moment, however it gives rise to no magnetostrictive strain and thus no magnetoacoustic emission. In contrast, magnetoacoustic emission is largest for 90° wall movements.[63] It has been proposed that different magnetoacoustic emission signals for different field directions may enable the principal stress axis to be identified. Unfortunately, magnetic methods are sensitive to both stress and the component microstructure (Fig. 9*b*), which must therefore be accounted for using calibration experiments.[64] Nevertheless, for materials which are magnetostrictive and are well characterised, magnetic methods provide cheap and portable methods for non-destructive residual stress measurement.

Eddy current techniques are based on inducing eddy currents in the material under test and detecting changes in the electrical conductivity or magnetic permeability through changes in the test coil impedance. The penetration depth (related to the skin depth) can be changed by altering the excitation frequency, but is around 1 mm at practical frequencies, and the probe cannot identify the direction of the applied stress. Recent work[65] looking at residual stresses in Ti–6Al–4V illustrates that eddy current methods can be applied to a wider range of materials than magnetic methods. Eddy current methods are not well suited to basic measurements of residual stress due to the sensitivity of eddy current monitoring to plastic work and microstructural changes, but they can provide a quick and cheap

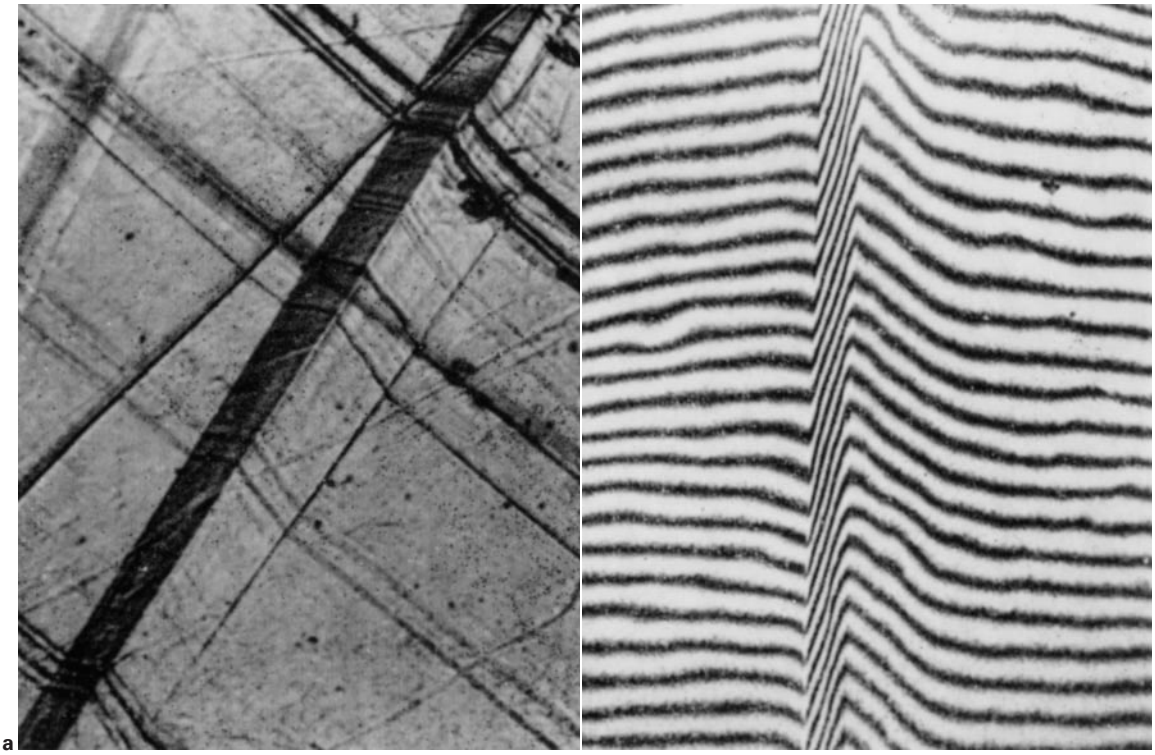

a accommodating shape deformations due to two adjacent plates of Widmanstätten ferrite: each component of tent-like relief is uniform, and scratches when deflected remain straight; *b* plastic accommodation adjacent to single plate of Widmanstätten ferrite: note how deformation within plate is uniform, but deformation in austenite causes Tolansky interference fringes to curve, with most intense accommodation adjacent to plate (After Ref. 91)

11 Transformation strains can be obtained by measuring displacements at free surfaces

in-line inspection method as part of an industrial quality control cycle.

ULTRASONICS

Changes in ultrasonic speed can be observed when a material is subjected to a stress,[66] the changes providing a measure of the stress averaged along the wave path. The acoustoelastic coefficients necessary for the analysis are usually calculated using calibration tests.[67] Different types of wave can be employed but the commonly used technique is the critically refracted longitudinal wave method. The greatest sensitivity is obtained when the wave propagates in the same direction as the stress. The stress can be calculated according to

$$\frac{V_{pp}-V_L^0}{V_L^0}=\bar{k}_1\sigma_p+\bar{k}_2(\sigma_q+\sigma_s)$$
$$\frac{V_{pq}-V_T^0}{V_T^0}=\bar{k}_3\sigma_p+\bar{k}_4\sigma_q+\bar{k}_5\sigma_s \quad \ldots\ldots\ldots (11)$$

where V_L^0 and V_T^0 are the isotropic longitudinal and transverse velocities, V_{ij} is the velocity of a wave travelling in direction i polarised in direction j, when the wave propagates in direction p, a principal stress direction; s is orthogonal to p and q; and $\bar{k}_i$ are the appropriate coupling constants.

The method provides a measure of the macrostresses over large volumes of material. Ultrasonic wave velocities can depend on microstructural inhomogeneities[68] and there are difficulties in separating the effects of multiaxial stresses. Nevertheless, being portable and cheap to undertake, the method is well suited to routine inspection procedures and industrial studies of large components, such as steam turbine discs.[66,69]

PIEZOSPECTROSCOPIC EFFECTS

Characteristic Raman or fluorescence luminescence lines shift linearly with variations in the hydrostatic stress. Samples which give good Raman spectra include silicon carbide and alumina–zirconia;[70] Cr^{3+} impurity containing alumina fibres are known to fluoresce under stress.[71,72]

The methods are useful because spectral shifts can be easily and accurately measured. By using optical microscopy, it is possible to select regions of interest just a few micrometres in size (Fig. 10). Furthermore, given the optical transparency of some matrix materials such as

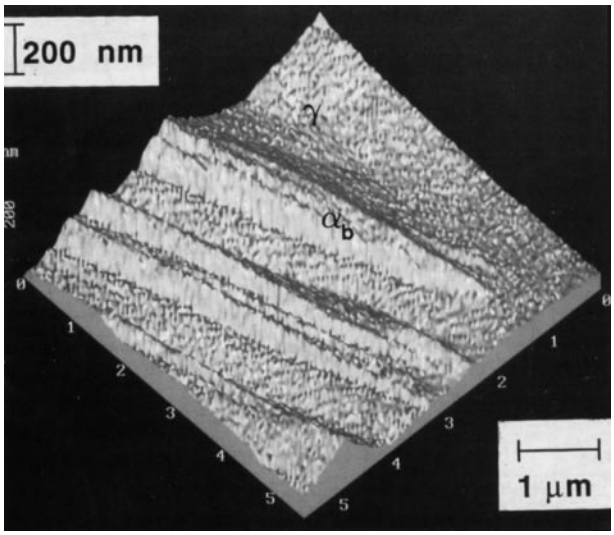

12 Atomic force microscope image showing surface relief due to individual bainite subunits, which all belong to tip of sheaf

epoxy,[73] or sapphire,[71] it is even possible to obtain subsurface information. Consequently, these methods are well suited to the study of fibre composites, providing basic information about the build up of stresses from fibre ends to centres[70,72,74] and to distinguish between micro- and macrostresses.[75,76]

THERMOELASTIC METHODS

The elastic deformation of a material causes small changes in temperature (1 mK for 1 MPa in steel). It is possible, using an appropriate infrared camera, to map the thermal variations giving an indication of concomitant variations in stress.[77,78] The thermoelastic constant β, which describes the dependence of temperature on stress, allows the hydrostatic stress component to be determined using the relation[79]

$$\text{heat} \approx -\beta \frac{\partial}{\partial T} (\sigma_{11}+\sigma_{22}+\sigma_{33}) \quad \ldots\ldots (12)$$

The effect is rather small relative to the sensitivity of the currently available infrared cameras and hence has limited use at present. It is well suited to fatigue studies.[80]

PHOTOELASTIC METHODS

The tendency for the speed of light in transparent materials to vary anisotropically when the material is subjected to a stress is termed the photoelastic effect. It gives rise to interference fringe patterns when such objects are viewed in white or monochromatic light between crossed polars. The resulting fringe patterns can be interpreted to give the local maximum shear stress if the stress optic coefficient n is known from a calibration experiment[81]

$$\sigma_{11}-\sigma_{22}=\frac{fn}{t} \quad \ldots\ldots\ldots\ldots (13)$$

where σ_{11}, σ_{22} are the in plane principal stresses, f is the fringe order, and t is the optical path length through the birefringent material. Photoelastic measurements are in general made using two-dimensional epoxy resin models or from slices cut from three-dimensional models in which the stresses have been frozen in. An example of a three-dimensional study is given in Ref. 82. Frequently, lacquers stuck to the surface of the component are monitored, for example, to examine a kitchen sink;[83] automated procedures have also been developed.[84] Residual strains arising from dislocation kink bands and long range plastic misfit stresses have been measured photoelastically in ionic AgCl model materials.[85,86] The deformation behaviour of AgCl resembles that of face centred cubic metals.

Measurement of transformation strains

Techniques for the characterisation of unconstrained transformation strains rely on observations made at free surfaces. A sample of the parent phase is prepared metallographically and transformed partially into the product phase. The resulting displacements at the free surface yield information about the stress free transformation strains.

The displacements can be measured by the deflection of fiducial marks (such as scratches, thermal grooves, slip lines) or using Tolansky interference microscopy (Fig. 11).[87–91] The measurements include the angle through which the specimen surface is tilted by transformation, and the angle between the habit plane trace and a scratch before and after transformation for more than a pair of non-collinear scratches. This helps to determine the displacement direction given the assumption that the shape strain is an invariant-plane strain. Many of the transformations of interest occur at relatively high temperatures. Dunne and Bowles[90] have described a technique in which an aluminous silicate fibre brush is used to hot scratch the surface; the advantage of deliberately scratching as opposed to using features such as thermal grooves is that it permits a larger number of non-parallel scratches to be measured.

There are cases where higher resolution is necessary, for fine transformation products. Figure 12 shows an atomic force microscope image of displacements caused during the formation of bainite;[92] the atomic force microscope essentially measures the topography of a surface, in principle to atomic resolution.

The scratch rotation technique has an accuracy of about $\pm 0{\cdot}5\%$, which is sometimes insufficient. Krauklis and Bowles[93] have used a dimensionally stable silver grid on untransformed parent phase to study transformation strains to a very high accuracy.

Summary

There are many methods for the characterisation of residual stress in engineering materials. Before selecting one method over another, it is important to consider the sampling volume characteristic of the technique and the types of stress (I, II, and III) which may be of importance. In many cases, much can be learnt from the complementary use of more than one technique.

References

1. P. J. WITHERS and H. K. D. H. BHADESHIA: *Mater. Sci. Technol.*, 2001, **17**, 366–375.
2. P. J. WITHERS, W. M. STOBBS, and O. B. PEDERSEN: *Acta Metall.*, 1989, **37**, 3061–3084.
3. K. OHNO, H. HARADA, T. YAMAGATA, M. YAMAZAKI, and K. OHSUMI: *Adv. X-Ray Anal.*, 1989, **32**, 363–374.
4. P. J. WITHERS: in 'Encyclopedia of materials science and technology', (ed. K. H. J. Buschow *et al.*); 2001, Oxford, Pergamon (to be published).
5. P. J. BOUCHARD: in 'Encyclopedia of materials science and technology', (ed. K. H. J. Buschow *et al.*), 2001, Oxford, Pergamon (to be published).
6. J. F. FLAVENOT: in 'Handbook of measurement of residual stresses', (ed. J. Lu), 35–48; 1996, Lilburn, GA, Society for Experimental Mechanics.
7. T. W. CLYNE and S. C. GILL: *J. Therm. Spray Technol.*, 1996, **5**, (4), 1–18.
8. S. KURODA, T. KUKUSHIMA, and S. KITAHARA: *J. Vac. Sci. Technol.*, 1987, **A5**, 72–87.
9. S. G. MALHOTRA, Z. U. REK, S. M. YALISOVE, and J. C. BILELLO: *Thin Solid Films*, 1997, **301**, 45–54.
10. J.-H. CHOI, H. G. KIM, and S.-G. YOON: *J. Mater. Sci.: Mater. Electron.*, 1992, **3**, 87–92.
11. S. GUNGOR and C. RUIZ: *Key Eng. Mater.*, 1997, **127**, 851–859.
12. M. P. I. M. EIJPE and P. C. POWELL: *J. Thermoplast. Compos. Mater.*, 1997, **10**, 334–352.
13. D. J. GREVING, E. F. RYBICKI, and J. R. SHADLEY: in 'Thermal spray industrial applications', Boston, MA, USA, June 1994; 1994, Materials Park, OH, ASM International.
14. S. C. GILL and T. W. CLYNE: *Thin Solid Films*, 1994, **250**, 172–180.
15. L. CHANDRA, M. CHOWALLA, G. A. J. AMARATUNGA, and T. W. CLYNE: *Diam. Relat. Mater.*, 1996, **5**, 674–681.
16. R. O. E. VIJGEN and J. H. DAUTZENBERG: *Thin Solid Films*, 1995, **270**, 264–269.
17. K. SASAKI, M. KISHIDA, and T. ITOH: *Exp. Mech.*, 1997, **37**, 250–257.
18. G. SCHAJER and M. TOOTOONIAN: *Exp. Mech.*, 1997, **37**, 299–306.
19. K. Y. LI: *Opt. Lasers Eng.*, 1997, **27**, 125–136.
20. A. MAKINO and D. NELSON: *J. Eng. Mater. Technol. (Trans. ASME)*, 1997, **119**, 95–103.
21. D. V. NELSON, A. MAKINO, and E. A. FUCHS: *Opt. Lasers Eng.*, 1997, **27**, 3–23.

22. G. SCHAJER: in 'Encyclopedia of materials science and technology', (ed. K. H. J. Buschow *et al.*); 2001, Oxford, Pergamon (to be published).
23. R. H. LEGGATT, D. J. SMITH, S. D. SMITH, and F. FAURE: *J. Strain Anal. Eng. Des.*, 1996, **31**, 177–186.
24. S. CHOI and L. BROUTMAN: *Polym. Lorea*, 1997, **21**, 71–82.
25. F. FAURE and R. H. LEGGATT: *Int. J. Pressure Vessels Piping*, 1996, **65**, 265–275.
26. P. PANTUCEK, E. LUGSCHEIDER, and U. MILLER: Proc. 2nd Plasma-Technik-Symposium, (ed. S. B. Sandmeier *et al.*), 143–150; 1991, Lucerne, Switzerland, Plasma Technik.
27. G. S. SCHAJER, G. ROY, M. T. FLAMAN, and J. LU: in 'Handbook of measurement of residual stresses', (ed. J. Lu), 5–34; 1996, Lilburn, GA, Society for Experimental Mechanics.
28. Y. Y. WANG and F. P. CHIANG: *Opt. Lasers Eng.*, 1997, **27**, 89–100.
29. W. CHENG, I. FINNIE, M. GREMAUD, A. ROSSELET, and R. D. STREIT: *J. Eng. Mater. Technol. (Trans. ASME)*, 1994, **116**, 556–560.
30. M. GREMAUD, W. CHENG, I. FINNIE, and M. B. PRIME: *J. Eng. Mater. Technol. (Trans. ASME)*, 1994, **116**, 550–555.
31. K. KOVAC: *J. Mater. Process. Technol.*, 1995, **52**, 503–514.
32. X. LI and K. HAYASHI: *Biorheology*, 1996, **33**, 439–449.
33. Y. UEDA: in 'Handbook of residual stress measurements', (ed. J. Lu), 49–70; 1996, Lilburn, GA, Society for Experimental Mechanics.
34. S. M. PICKARD, D. B. MIRACLE, B. S. MAJUMDAR, K. L. KENDIG, L. ROTHENFLUE, and D. COKER: *Acta Metall. Mater.*, 1995, **43**, (8), 3105–3112.
35. M. B. PRIME and A. R. GONZALES: Proc. 6th Int. Conf. on 'Residual stresses', Oxford, UK, July 2000 (ed. G. A. Webster), Vol. 1, 617–624; 2000, London, IoM Communications.
36. A. D. KRAWITZ, R. A. WINHOLTZ, and C. M. WEISBROOK: *Mater. Sci. Eng. A*, 1996, **206**, 176–182.
37. D. S. KUPPERMAN, S. MAJUMDAR, J. P. SINGH, and A. SAIGAL: in 'Measurement of residual and applied stress using neutron diffraction', (ed. M. T. Hutchings and A. D. Krawitz), 439–450; 1992.
38. P. J. WITHERS: *Key Eng. Mater.: Ceram. Matrix Compos.*, 1995, **108–110**, 291–314.
39. B. D. CULLITY: 'Elements of X-ray diffraction', 2 edn; 1978, New York, Addison-Wesley.
40. B. CLAUSEN, T. LORENTZEN, and T. LEFFERS: *Acta Mater.*, 1998, **46**, 3087–3098.
41. A. N. EZEILO, G. A. WEBSTER, P. J. WEBSTER, and X. WANG: *Physica B: Phys. Condens. Matter*, 1992, **180**, 1044–1046.
42. T. LORENTZEN and T. LEFFERS: in 'Measurement of residual and applied stress using neutron diffraction', Vol. 216, NATO ASI Series E (ed. M. T. Hutchings and A. D. Krawitz), 253–261; 1992, Dordrecht, Kluwer.
43. M. FRANXOIS, J. M. SPRAUEL, C. F. DEHAN, M. R. JAMES, F. CONVERT, J. LU, J. L. LEBRUN, N. JI, and R. W. HENDRICKS: in 'Handbook of measurement of residual stresses', (ed. J. Lu), 71–131; 1996, Lilburn, GA, Society for Experimental Mechanics.
44. C. J. HUMPHREYS and E. G. BITHELL: in 'Electron diffraction techniques', (ed. J. M. Cowley), 75–151; 1992, Oxford, Oxford University Press.
45. R. C. ECOB, R. A. RICKS, and A. J. PORTER: *Scr. Metall.*, 1982, **31**, 1085–1088.
46. V. RANDLE and B. RALPH: *J. Microsc.*, 1987, **14**, 305–312.
47. M. FAHRMANN, J. G. WOLF, and T. M. POLLOCK: *Mater. Sci. Eng. A*, 1996, **A210**, 8–15.
48. A. J. WILKINSON: Proc. 6th Int. Conf. on 'Residual stresses', Oxford, UK, July 2000, (ed. G. A. Webster), Vol. 1, 625–632; 2000, London, IoM Communications.
49. M. R. WATTS and P. J. WITHERS: Proc. 11th Int. Conf. on 'Composite materials', Gold Coast, August 1997, (ed. M. L. Scott *et al.*), Vol. 3, 1821–1831; 1997, Letchworth, Herts, Woodhead Publishing.
50. H. MOHRBACHER, K. VANACKER, B. BLANPAIN, P. VANHOUTTE, and J. P. CELIS: *J. Mater. Res.*, 1996, **7**, 1776–1782.
51. W. C. MARRA, P. EISENBERGER, and A. Y. CHIO: *J. Appl. Phys.*, 1979, **50**, 627.
52. M. R. DAYMOND, M. A. M. BOURKE, R. V. DREELE, B. CLAUSEN, and T. LORENTZEN: *J. Appl. Phys.*, 1997, **82**, 1554–1556.
53. P. J. WTHERS, M. W. JOHNSON, and J. S. WRIGHT: *Physica B: Phys. Condens. Matter*, 2000, **292**, 273–285.
54. S. SPOONER and X. L. WANG: *J. Appl. Crystallogr.*, 1997, **30**, 449–455.
55. M. R. DAYMOND and P. J. WITHERS: *Scr. Mater.*, 1996, **35**, 1229–1234.
56. J. L. LEBRUN, P. GERGAUD, V. JI, and M. BELASSEL: *J. Phys. (France) IV*, 1995, **4**, 265–268.
57. P. J. WEBSTER, G. MILLS, X. D. WANG, W. P. KANG, and T. M. HOLDEN: *J. Neutr. Res.*, 1996, **3**, 223–240.
58. P. J. WITHERS and P. J. WEBSTER: *Strain*, 2001, **37**, 19–33.
59. H. F. POULSEN, T. LORENTZEN, R. FEIDENHANSL, and Y. L. LIU: *Metall. Mater. Trans. A*, 1997, **28A**, 237–243.
60. W. REIMERS, M. BRODA, G. DANTZ, K.-D. LISS, A. PYZALA, T. SCHMAKERS, and T. TSCHENSCHER: *J. Nondestr. Eval.*, 1998, **17**, (3), 129–140.
61. S. ABUKU: *Jpn J. Appl. Phys.*, 1977, **16**, 1161–1170.
62. D. J. BUTTLE and C. B. SCRUBY: in 'Encyclopedia of materials science and technology', (ed. K. H. J. Buschow *et al.*); 2001, Oxford, Pergamon (to be published).
63. D. J. BUTTLE, C. B. SCRUBY, G. A. D. BRIGGS, and J. P. JAKUBOVICS: *Proc. R. Soc. A*, 1987, **414**, 469–497.
64. S. TIITTO: in 'Handbook of measurement of residual stresses', (ed. J. Lu); 179–224; 1996, Lilburn, GA, Society for Experimental Mechanics.
65. F. C. SCHOENIG, J. A. SOULES, H. CHANG, and J. J. DICELLO: *Mater. Eval.*, 1995, **53**, 22–26.
66. R. E. GREEN: in 'Treatise on materials science and technology', Vol. 3, 73; 1973, New York, Academic Press.
67. R. B. THOMPSON, W. Y. LU, and A. V. CLARK: in 'Handbook of measurement of residual stresses', (ed. J. Lu), 149–178; 1996, Lilburn, GA, Society for Experimental Mechanics.
68. R. B. THOMPSON, J. F. SMITH, and S. S. LEE: in 'Non-destructive evaluation, application to materials processing', (ed. O. Buck and S. M. Wolf), 137–145; 1984, Metals Park, OH, American Society for Metals.
69. D. E. BRAY, N. PATHAK, and M. N. SRINIVASAN: *Mater. Sci. Forum*, 1997, **210**, 317–324.
70. X. YANG and R. J. YOUNG: *Composites*, 1994, **25**, 488–493.
71. M. A. QING and D. R. CLARKE: *Acta Metall. Mater.*, 1993, **41**, 1817–1823.
72. M. A. QING, L. C. LIANG, D. R. CLARKE, and J. W. HUTCHINSON: *Acta Metall. Mater.*, 1994, **42**, 3299–3308.
73. I. M. ROBINSON, R. J. YOUNG, C. GALIOTIS, and D. N. BATCHELDER: *J. Mater. Sci.*, 1987, **22**, 3642.
74. L. S. SCHADLER and C. GALIOTIS: *Int. Mater. Rev.*, 1995, **40**, 116–134.
75. V. SERGO, D. M. LIPKIN, G. DePORTU, and D. R. CLARKE: *J. Am. Ceram. Soc.*, 1997, **80**, 1633–1638.
76. Q. MA and D. R. CLARKE: *J. Am. Ceram. Soc.*, 1993, **76**, (6), 1433–1440.
77. S. OFFERMANN, C. BISSIEUX, and J. L. BEAUDOIN: *Res. Nondestr. Eval.*, 1993, **7**, 239–251.
78. P. STANLEY: in 'Encyclopedia of materials science and technology', (ed. K. H. J. Buschow *et al.*); 2001, Oxford, Pergamon (to be published).
79. D. S. MOUNTAIN and J. M. B. WEBBER: *Proc. Soc. Photo-Opt. Inst. Eng.*, 1978, **164**, 189–196.
80. N. HARWOOD and W. M. CUMMINGS (eds.): in 'Thermoelastic stress analysis'; 1991, Bristol, IOP Publishing (Adam Hilger).
81. E. A. PATTERSON: in 'Encyclopedia of materials science and technology', (ed. K. H. J. Buschow *et al.*); 2001, Oxford, Pergamon (to be published).
82. A. PAWLAK and A. GALESKI: *Polym. Eng. Sci.*, 1996, **36**, 2727–2735.
83. T. W. CORBY and W. E. NICKOLA: *Opt. Lasers Eng.*, 1997, **27**, 111–123.
84. A. AJOVALASIT, S. BARONE, and G. PETRUCCI: *J. Strain Anal.*, 1998, **33**, 75–91.
85. M. J. STOWELL: *Philos. Mag.*, 1962, **7**, 677–704.
86. J. F. NYE, R. D. SPENCE, and M. J. SPRACKLING: *Philos. Mag.*, 1957, **2**, 722–776.
87. J. S. BOWLES and A. J. MORTON: *Acta Metall.*, 1964, **12**, 629–673.
88. A. J. MORTON and C. M. WAYMAN: *Acta Metall.*, 1966, **14**, 1567–1581.
89. E. J. EFSIC and C. M. WAYMAN: *Trans. AIME*, 1967, **239**, 873–882.
90. D. P. DUNNE and J. S. BOWLES: *Acta Metall.*, 1969, **17**, 201–212.
91. J. D. WATSON and P. G. McDOUGALL: *Acta Metall.*, 1973, **21**, 961–973.
92. E. SWALLOW and H. K. D. H. BHADESHIA: *Mater. Sci. Technol.*, 1996, **12**, 121–125.
93. P. KRAUKLIS and J. S. BOWLES: *Acta Metall.*, 1969, **17**, 997–1004.